Surface mode hybridization in the optical response of core-shell particles

E. Thiessen, R. L. Heinisch, F. X. Bronold, and H. Fehske
Institut für Physik, Ernst-Moritz-Arndt-Universität Greifswald, 17489 Greifswald, Germany
(Received 29 July 2015; revised manuscript received 12 February 2016; published 11 March 2016)

We present an exact rewriting of the Mie coefficients describing the scattering of light by a spherical core-shell particle which enables their interpretation in terms of a hybridization of the two surface modes arising, respectively, at the core-shell and the shell-medium interface. For this particular case, we thus obtain from the Mie theory—analytically for all multipole orders and hence for arbitrarily sized particles—the hybridization scenario, which so far has been employed primarily for small particles in the electrostatic approximation. To demonstrate the strength of the rewriting approach, we also extract the hybridization scenario for a stratified sphere directly from the expansion coefficients for the electromagnetic fields.

DOI: 10.1103/PhysRevA.93.033827

I. INTRODUCTION

Ever since the pioneering work by Mie [1] and Debye [2], the classical optical response of objects has played an important role in applied science [3,4]. The applications range from the spectroscopy of grains embedded in gaseous interstellar environments [5] to plasmonic devices on the nanoscale [6,7]. In particular, the latter is a growing field of research driven by the progress in materials synthesis and processing [8], which provides plasmonic nanostructures of continuously increasing complexity [9,10]: nanorice [11], nanorings [12], or nanoshells [13,14], to name only a few. The geometry of these structures provides an efficient means to tailor their optical response, opening thereby new fields of application, for instance, in biomedicine [15] or photovoltaics [16], which in turn stimulate the design of even more intricate structures.

Different methods have been developed over the years to analyze light scattering by composite objects. While the approaches [17–24] extending the early analytical works [1,2] are usually restricted to spherical particles, numerical approaches are now available which do not suffer this limitation [25–27]. Depending on the discretization, the methods are either surface or volume based. In particular, the latter are very powerful since they can handle arbitrarily shaped inhomogeneous objects. But like the generalizations of Mie's original approach, numerical methods do not provide a physical picture of the interaction of light with composite objects.

An appealing physical picture was first given by Prodan and co-workers [28,29] for metallic nanoshells and later by Preston and Signorell [30] for dielectric core-shell particles. As pointed out by these authors, the optical response of composite entities such as nanoshells can be understood within the surface mode hybridization scenario. The essence of the scenario is that the surface modes arising at the interfaces of these objects interact with each other and result in optical resonances not to be found in homogeneous objects. Modification of the object's geometry changes the interaction and hence the optical response. Prodan and co-workers showed that the interaction can be interpreted as a kind of hybridization. In analogy to electronic states of condensed matter, optical resonances of composite objects can thus be labeled bonding and antibonding depending on their symmetry. Both Prodan and co-workers [28] and Preston and Signorell [30] worked out the hybridization scenario within the electrostatic approximation using, respectively, a Lagrangian and an eigenvalue method for the description of the charges induced at the interfaces of the object. The two approaches are very flexible, can be applied to arbitrary geometry, and do not necessarily require bulk dielectric functions. They can be combined with microscopic models for the optical response of the atomic constituents of the objects and are thus well suited for applications in nanoplasmonics [9,10].

The interpretation of light scattering by composite objects in terms of the hybridization scenario is often referred to as a new conceptual approach [31] or as a fundamentally different way of thinking about plasmonic effects [32]. As the Mie theory is the exact analytical description of light scattering by spheres and thus naturally includes all observed effects, the question arises whether the hybridization scenario can also be found directly in the Mie formulas and thus whether the new thinking can be united with the old formalism.

In this paper, we show that this is indeed the case. For the particular case of a spherical core-shell particle, the hybridization scenario can be straightforwardly derived from the Mie theory by recasting the Mie coefficients [3,4,17,33] in a form resembling the diagonal elements of a matrix resolvent describing two hybridized energy levels. The derivation, valid for all multipole orders and thus applicable to arbitrarily sized particles, starts with a splitting of the electromagnetic fields inside the shell into two parts [23,24], corresponding to the penetrating fields of a homogeneous particle made out of shell material and the scattering fields of a cavity filled with core material and sitting inside a homogeneous domain of shell material. In a second step, the expansion coefficients obtained by enforcing the boundary conditions at the core-shell and shell-medium interface are then rewritten into the desired form. The reorganization of the fields inside the shell and the reordering of the expansion coefficients it leads to yield no physical concepts beyond the hybridization scenario [28–30]. In fact, it was inspired by it. But it is comforting to see the scenario emerge directly from the formulas of the Mie theory, which are notoriously difficult to interpret. We thereby also generalize the work of Ruppin [19] and Uberoi [20] who showed, again only in the electrostatic approximation, that the optical response of a core-shell particle arises from two coupled subsystems. The hybridization scenario can also be found in the Mie formulas for a stratified sphere. Again, the splitting of the fields into penetrating and scattered parts and

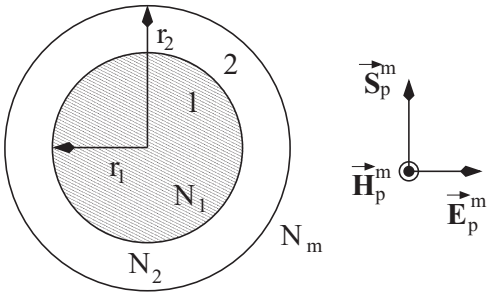

FIG. 1. Geometry of light scattering by a core-shell particle with total radius r_2 and core radius r_1 embedded in a medium. Refractive indices N_i characterize the core ($i = 1$), the shell ($i = 2$), and the medium $i = m$. The incident electromagnetic plane wave is described by a Poynting vector $\vec{S}_{\rm in}$ propagating in the z direction, an electric field $\vec{E}_{\rm p}^{\,m}$ polarized in the x direction, and a magnetic field $\vec{H}_{\rm p}^{\,m}$ along the y direction.

the reorganization of the expansion coefficients guided by the structure of the diagonal elements of a matrix resolvent describing hybridized energy levels are essential.

In the next section, we rewrite the Mie coefficients for a spherical core-shell particle and demonstrate how the building blocks of the hybridization scenario, i.e., the medium-embedded homogeneous shell particle and the shell-embedded core cavity, can be extracted from these expressions. For illustration, we present in Sec. III numerical results for a dielectric core-shell particle, the type of particle we suggested to employ in a gas discharge as an electric probe with optical read out [34]. In particular we show, up to the hexapole, data for the splitting between the bonding and antibonding resonances as well as the electric fields inside the particle. The stratified spherical particle is discussed separately in the Appendix. Concluding remarks are given in Sec. IV.

II. THEORY

The Mie theory [1,2] of light scattering by a spherical core-shell particle was worked out by Aden and Kerker [17] long ago. It can be found in many textbooks [3,4]. The geometry of the electromagnetic scattering problem is shown in Fig. 1. An electromagnetic wave with wave number λ^{-1} propagating in the z direction and an electric field polarized in the x direction hits a particle centered in the origin of the coordinate system. The particle with total radius r_2 and refractive index $N_2(\lambda^{-1}) = \sqrt{\varepsilon_2(\lambda^{-1})}$ contains a core with radius $r_1 = f r_2$ and refractive index $N_1(\lambda^{-1}) = \sqrt{\varepsilon_1(\lambda^{-1})}$, where $\varepsilon_{1,2}(\lambda^{-1}) = \varepsilon'_{1,2}(\lambda^{-1}) + i\varepsilon''_{1,2}(\lambda^{-1})$ are the complex dielectric functions for the two regions and $0 \leqslant f \leqslant 1$ is the filling factor. In the formulas below, we use $\kappa = 2\pi\lambda^{-1}$ and $\omega = 2\pi c\lambda^{-1}$ instead of λ^{-1} and ν, with c the speed of light, the abbreviations $k_i = \kappa N_i$ with $i = 1,2,m$, where N_m is the refractive index of the surrounding medium, and the size parameters $x_2 = 2\pi\lambda^{-1} r_2$ and $x_1 = 2\pi\lambda^{-1} r_1$.

In order to obtain the classical optical response of the particle, we expand, as in the standard procedure, the electromagnetic fields outside and inside the particle in the vector spherical harmonics $\vec{M}, \vec{N}$ and determine the expansion coefficients from the boundary conditions at the two interfaces [3,4,17]. Special attention is, however, paid to the shell region, where we follow Xu [23] and Peña and Pal [24] and split the fields in a manner suitable to bring out the hybridization scenario.

The expansions for the incident fields read [4]

$$\vec{E}_{\rm p}^{\,m} = \sum_{n=1}^{\infty} E_n \left(\vec{M}_{o1n}^{(1)} - i\vec{N}_{e1n}^{(1)}\right), \tag{1}$$

$$\vec{H}_{\rm p}^{\,m} = -\frac{k_m c}{\omega\mu_m} \sum_{n=1}^{\infty} E_n \left(\vec{M}_{e1n}^{(1)} + i\vec{N}_{o1n}^{(1)}\right), \tag{2}$$

with expansion coefficients

$$E_n = i^n E_0 \frac{2n+1}{n(n+1)}, \tag{3}$$

where E_0 is the strength of the incident electric field. The radial dependence of these fields is described by Bessel functions of the first kind, indicated by the superscript (1); thus they can be interpreted as the penetrating fields (explaining the subscript p) in the surrounding medium ($i = m$). The scattered fields outside the particle may be written as

$$\vec{E}_{\rm s}^{\,m} = \sum_{n=1}^{\infty} E_n \left(i a_n^m \vec{N}_{e1n}^{(3)} - b_n^m \vec{M}_{o1n}^{(3)}\right), \tag{4}$$

$$\vec{H}_{\rm s}^{\,m} = \frac{k_m c}{\omega\mu_m} \sum_{n=1}^{\infty} E_n \left(i b_n^m \vec{N}_{o1n}^{(3)} + a_n^m \vec{M}_{e1n}^{(3)}\right). \tag{5}$$

The superscript (3) indicates that Hankel functions of the first kind, $h_n = j_n + \mathrm{i} y_n$, are used for the radial dependence of the fields, whereby y_n are Bessel functions of the second kind, which will be indicated by the superscript (2). Inside the particle, the core and the shell regions have to be distinguished. The penetrating fields inside the core ($i = 1$) are given by

$$\vec{E}_{\rm p}^{\,1} = \sum_{n=1}^{\infty} E_n \left(c_n^1 \vec{M}_{o1n}^{(1)} - i d_n^1 \vec{N}_{e1n}^{(1)}\right), \tag{6}$$

$$\vec{H}_{\rm p}^{\,1} = -\frac{k_1 c}{\omega\mu_1} \sum_{n=1}^{\infty} E_n \left(d_n^1 \vec{M}_{e1n}^{(1)} + i c_n^1 \vec{N}_{o1n}^{(1)}\right), \tag{7}$$

and the fields inside the shell may be expressed as

$$\vec{E}_{\rm shell} = \sum_{n=1}^{\infty} E_n \left(f_n \vec{M}_{o1n}^{(1)} - i g_n \vec{N}_{e1n}^{(1)} + v_n \vec{M}_{o1n}^{(2)} - i w_n \vec{N}_{e1n}^{(2)}\right), \tag{8}$$

$$\vec{H}_{\rm shell} = -\frac{k_2 c}{\omega\mu_2} \sum_{n=1}^{\infty} E_n \left(g_n \vec{M}_{e1n}^{(1)} + i f_n \vec{N}_{o1n}^{(1)} + w_n \vec{M}_{e1n}^{(2)} + i v_n \vec{N}_{o1n}^{(2)}\right). \tag{9}$$

The expansions (8) and (9) going back to Aden and Kerker [17] are the basis of most applications of the Mie theory to spherical core-shell particles. In our previous work, we also used them [33,34]. Their physical content, however, is not obvious. To bring the physics to the forefront, it is more appropriate to follow the hybridization scenario [28–30] and

to express the fields inside the shell ($i = 2$) as follows [23,24]:

$$\vec{E}_{\rm shell} = \vec{E}_{\rm s}^{\,2} + \vec{E}_{\rm p}^{\,2} \quad \text{and} \quad \vec{H}_{\rm shell} = \vec{H}_{\rm s}^{\,2} + \vec{H}_{\rm p}^{\,2}, \tag{10}$$

where $\vec{E}_{\rm s}^{\,2}, \vec{H}_{\rm s}^{\,2}$ and $\vec{E}_{\rm p}^{\,2}, \vec{H}_{\rm p}^{\,2}$ are, respectively, the scattered fields (explaining the subscript s) of a cavity consisting of core material and embedded in a homogeneous domain of shell material and the penetrating fields of a homogeneous particle made out of shell material (hence the subscript p) embedded in the medium. Adopting Eqs. (4)–(5) and Eqs. (6)–(7) to the shell region results in

$$\vec{E}_{\rm s}^{\,2} = \sum_{n=1}^{\infty} E_n \left(i a_n^2 \vec{N}_{e1n}^{(3)} - b_n^2 \vec{M}_{o1n}^{(3)} \right), \tag{11}$$

$$\vec{H}_{\rm s}^{\,2} = \frac{k_2 c}{\omega \mu_2} \sum_{n=1}^{\infty} E_n \left(i b_n^2 \vec{N}_{o1n}^{(3)} + a_n^2 \vec{M}_{e1n}^{(3)} \right) \tag{12}$$

and

$$\vec{E}_{\rm p}^{\,2} = \sum_{n=1}^{\infty} E_n \left(c_n^2 \vec{M}_{o1n}^{(1)} - i d_n^2 \vec{N}_{e1n}^{(1)} \right), \tag{13}$$

$$\vec{H}_{\rm p}^{\,2} = -\frac{k_2 c}{\omega \mu_2} \sum_{n=1}^{\infty} E_n \left(d_n^2 \vec{M}_{e1n}^{(1)} + i c_n^2 \vec{N}_{o1n}^{(1)} \right). \tag{14}$$

Since the total number of expansion coefficients is unchanged, remaining in total eight, $a_n^m, b_n^m, a_n^2, b_n^2, c_n^2, d_n^2, c_n^1$, and d_n^1, the shell-medium boundary conditions at $r = r_2$,

$$\vec{r} \times \left(\vec{E}_{\rm p}^{\,m} + \vec{E}_{\rm s}^{\,m} - \vec{E}_{\rm s}^{\,2} - \vec{E}_{\rm p}^{\,2} \right) = 0, \tag{15}$$

$$\vec{r} \times \left(\vec{H}_{\rm p}^{\,m} + \vec{H}_{\rm s}^{\,m} - \vec{H}_{\rm s}^{\,2} - \vec{H}_{\rm p}^{\,2} \right) = 0, \tag{16}$$

and the core-shell boundary conditions at $r = r_1$,

$$\vec{r} \times \left(\vec{E}_{\rm s}^{\,2} + \vec{E}_{\rm p}^{\,2} - \vec{E}_{\rm p}^{\,1} \right) = 0, \tag{17}$$

$$\vec{r} \times \left(\vec{H}_{\rm s}^{\,2} + \vec{H}_{\rm p}^{\,2} - \vec{H}_{\rm p}^{\,1} \right) = 0, \tag{18}$$

are sufficient for their determination. For the derivation of the hybridization scenario, we focus on the coefficients d_n^2 and a_n^2, which are resonant for small particles up to fourth multipole order (as are all coefficients in front of the spherical vector harmonics $\vec{N}_{e1}$).

The hybridization scenario becomes apparent by writing the expansion coefficients d_n^2 and a_n^2 in a form resembling the diagonal elements of a matrix resolvent,

$$G(E) = \begin{pmatrix} \varepsilon_A - E & V \\ V^* & \varepsilon_B - E \end{pmatrix}^{-1}, \tag{19}$$

describing the hybridization of two energy levels ε_A and ε_B. The basis for this matrix are the states $|A\rangle$ and $|B\rangle$. Let us consider

$$\begin{aligned} G_A(E) &= \langle A|G(E)|A\rangle \\ &= \frac{1}{g_A^{-1}(E) - \dfrac{|V|^2}{g_B^{-1}(E)}} \end{aligned} \tag{20}$$

as a guide, where $|V|^2$ is the hybridization strength of the two levels and $g_i(E) = (E - \varepsilon_i)^{-1}$ is the resolvent of the isolated level $i = A, B$. The pole of $g_i(E)$ gives the energy of the noninteracting level i, while the two poles of $G_A(E)$ are the excitation energies of the interacting system. Once the coefficients are in this form, their interpretation in terms of a hybridization scenario is thus obvious.

Indeed, the coefficients d_n^2 and a_n^2 obtained from the boundary conditions (15)–(18) can be written as

$$d_n^2 = \frac{X_n^2(x_2)}{E_n^2(x_2) - \dfrac{X_n^{\rm cp1}(x_1) Z_n^2(x_2)}{E_n^1(x_1)}} \tag{21}$$

and

$$a_n^2 = \frac{X_n^{\rm cp1}(x_1) X_n^2(x_2)/E_n^2(x_2)}{E_n^1(x_1) - \dfrac{X_n^{\rm cp1}(x_1) Z_n^2(x_2)}{E_n^2(x_2)}}, \tag{22}$$

with E_n^1, E_n^2, and $X_n^{\rm cp1} Z_n^2$ playing the role of g_A^{-1}, g_B^{-1}, and $|V|^2$, respectively. The function X_n^2 has no direct analog. For better readability, we postpone the definitions of these functions to the point where they enter the discussion of the physical content of Eqs. (21) and (22).

A comparison of (21) and (22) with (20) suggests, now at the level of the Mie coefficients, that the optical response of a core-shell particle is the response of two hybridized subsystems, with individual resonances determined by

$$\begin{aligned} E_n^2(x_2) &= N_2 \xi_n'(N_m x_2) \psi_n(N_2 x_2) - N_m \xi_n(N_m x_2) \psi_n'(N_2 x_2) \\ &= 0 \end{aligned} \tag{23}$$

and

$$\begin{aligned} E_n^1(x_1) &= N_1 \xi_n'(N_2 x_1) \psi_n(N_1 x_1) - N_2 \xi_n(N_2 x_1) \psi_n'(N_1 x_1) \\ &= 0, \end{aligned} \tag{24}$$

respectively, and a hybridization strength given by $X_n^{\rm cp1}(x_1) Z_n^2(x_2)$. We have chosen all components to be nonmagnetic ($\mu_{1,2,m} = 1$). Notice in Eqs. (23) and (24) the Ricatti-Bessel functions $\psi_n(\rho) = \rho j_n(\rho)$ and $\xi_n(\rho) = \rho h_n(\rho)$ as well as the implicit definitions of the functions E_n^2 and E_n^1 appearing in (21) and (22). The physical content of (23) and (24) can be deduced by comparing these equations with the denominator of the scattering coefficient describing a homogeneous particle [4],

$$a_n^m = \frac{N_1 \psi_n'(N_m x) \psi_n(N_1 x) - N_m \psi_n(N_m x) \psi_n'(N_1 x)}{N_1 \xi_n'(N_m x) \psi_n(N_1 x) - N_m \xi_n(N_m x) \psi_n'(N_1 x)}, \tag{25}$$

which has to vanish in the resonance case. Here, N_1 and N_m are the refractive indices of the particle and the surrounding medium, respectively, and x is the size parameter of the particle. Clearly, Eq. (23) is the resonance condition of a homogeneous particle with size parameter x_2 and refractive index N_2 embedded in a medium specified by N_m, while Eq. (24) is the resonance condition of a homogeneous particle with size parameter x_1 and refractive index N_1 embedded in a medium characterized by N_2. If the real part of the dielectric function of the core $\varepsilon_1' > 0$ and the real part of the dielectric function of the shell $\varepsilon_2' < 0$, then it is, however,

the embedding medium which supports the surface modes. It is thus appropriate to consider (24) as the resonance condition of a cavity filled with material described by N_1 and embedded in a medium characterized by N_2.

So far, we extracted from the Mie formulas the two elementary building blocks, i.e., a shell-embedded core cavity and a medium-embedded homogeneous shell particle, whose surface modes hybridize to make up the optical response of the core-shell particle. We now turn to the hybridization strength $X_n^{\mathrm{cp1}}(x_1)Z_n^2(x_2)$. It is interesting to analyze under what conditions it vanishes and what this implies for the expansion coefficients. The two subsystems are noninteracting when at least one of the following conditions holds:

$$\begin{aligned} X_n^{\mathrm{cp1}}(x_1) &= N_1\psi_n(N_2x_1)\psi_n'(N_1x_1) - N_2\psi_n'(N_2x_1)\psi_n(N_1x_1) \\ &= 0, \end{aligned} \tag{26}$$

$$\begin{aligned} Z_n^2(x_2) &= N_2\xi_n'(N_mx_2)\xi_n(N_2x_2) - N_m\xi_n(N_mx_2)\xi_n'(N_2x_2) \\ &= 0. \end{aligned} \tag{27}$$

Condition (26), which implicitly defines X_n^{cp1}, is satisfied when the refractive indices of the core and the shell are the same, $N_1 = N_2$. It leads to $a_n^2 = 0$ and

$$\begin{aligned} d_n^2 &= \frac{X_n^2(x_2)}{E_n^2(x_2)} \\ &= \frac{N_2\xi_n'(N_mx_2)\psi_n(N_mx_2) - N_2\xi_n(N_mx_2)\psi_n'(N_mx_2)}{N_2\xi_n'(N_mx_2)\psi_n(N_2x_2) - N_m\xi_n(N_mx_2)\psi_n'(N_2x_2)} \\ &= d_n^1, \end{aligned} \tag{28}$$

where d_n^1 is the coefficient arising in the expansions (6) and (7) for the penetrating fields inside the core, which is now identical with the shell. Note that the numerator in the second equality defines the function X_n^2 appearing in Eqs. (21) and (22). Thus, due to the absence of the core-shell interface, the scattering fields in the shell region vanish, leading to $a_n^2 = 0$, and the penetrating fields inside the shell become equivalent to the penetrating fields of the core, signalled by $d_n^2 = d_n^1$, with expansion coefficients describing the fields inside a homogeneous particle with refractive index N_2 embedded in a medium with refractive index N_m. The core-shell particle is in this limit reduced to a medium-embedded homogeneous shell particle.

The second condition (27), which implicitly defines Z_n^2, reduces the core-shell particle to a cavity embedded in a homogeneous medium. In this case, the refractive indices of the medium and the shell have to be identical, $N_m = N_2$, leading to $d_n^2 = 1$ and

$$a_n^2 = \frac{N_1\psi_n'(N_2x_1)\psi_n(N_1x_1) - N_2\psi_n(N_2x_1)\psi_n'(N_1x_1)}{N_1\xi_n'(N_2x_1)\psi_n(N_1x_1) - N_2\xi_n(N_2x_1)\psi_n'(N_1x_1)}. \tag{29}$$

Hence, due to the missing medium-shell interface, the penetrating fields of the shell become equal to the incoming fields, which are considered to be the penetrating fields in the medium, as can be seen by comparing Eqs. (13) and (14) for $d_n^2 = 1$ with Eqs. (1) and (2). The expansion coefficient a_n^2 is in this limit attached to the scattered fields of a cavity. Indeed, looking at the scattering coefficient of a homogeneous sphere [4] a_n^m given by Eq. (25) and substituting $N_m \to N_2$ and $x \to x_1$ makes (25) identical to (29). Hence, for $N_m = N_2$, the core-shell particle is reduced to a core cavity embedded in a shell medium.

It should be noted that in the standard expansion, the coefficients f_n, g_n, v_n, and w_n reduce in the respective limits also to the Mie coefficients of a medium-embedded homogeneous shell particle and a shell-embedded core cavity [33]. What we have shown by working with a_n^2, b_n^2, c_n^2, and d_n^2 and rewriting them in a particular manner is that the two limiting cases are actually two building blocks whose resonances are always virtually present. They are encoded in the functions $E_n^2(x_2)$ and $E_n^1(x_1)$. The interaction $X_n^{\mathrm{cp1}}(x_1)Z_n^2(x_2)$, controlled by the geometry and the material parameters, defines their lifetimes and makes the optical response of the core-shell particle given by the poles of d_n^2 and a_n^2 unique, in full accordance with the hybridization scenario [28–30].

Before presenting numerical results for finite hybridization strength, let us consider the case where the hybridization is turned off by a vanishing filling factor $f = r_1/r_2 = x_1/x_2$. Depending on how the limit $f \to 0$ is taken, the core-shell particle reduces again to either one of its building blocks: a medium-embedded homogeneous shell particle or a shell-embedded core cavity. If the filling factor vanishes because the core becomes smaller and smaller, that is, because $x_1 \to 0$, while x_2 is fixed, it is $X_n^{\mathrm{cp1}}(x_1)$ which vanishes. As discussed above, the core-shell particle is then reduced to a homogeneous particle made out of shell material and embedded in a medium characterized by a refractive index N_m. If the filling factor vanishes, however, because the particle becomes larger and larger while the core size is fixed, that is, for x_1 fixed and $x_2 \to \infty$, it is $Z_n^2(x_2)$ which vanishes and reduces, according to the discussion given in the previous paragraph, the core-shell particle to a cavity made out of core material embedded in a homogeneous surrounding made out of shell material. For finite filling factors, both $X_n^{\mathrm{cp1}}(x_1)$ and $Z_n^2(x_2)$ are finite and mix the optical response of the building blocks. This will be discussed in the next section.

The reorganization of the Mie theory discussed in this section for the particular case of a spherical core-shell particle can be applied to other composite particles as well, provided the symmetry is high enough to yield analytical expressions for the expansion coefficients of the electromagnetic fields. In the Appendix, we show this for a stratified sphere [18,21–23].

III. ILLUSTRATION

To illustrate the classical optical response of a spherical core-shell particle, we consider a particle with a dielectric core and a dielectric shell. Previously, we proposed to use this type of particle in a gas discharge as an electric probe with optical read out [34]. The idea, formulated initially for a homogeneous dielectric particle [35], is to determine the electric field at the particle's position in the discharge from the balance of the forces acting on it and the charge-dependent shift of one of its extinction resonances. The shifts can be maximized by localizing inside the shell the elementary charges the particle acquired from the plasma using materials with negative electron affinity as a core and materials with positive electron affinity as a shell.

TABLE I. Parameters for the model core-shell particle.

Model	λ_{TO}^{-1} (cm^{-1})	ε_0	ε_∞
Core	300	3	2
Shell	600	20	2

The extinction spectra we calculated with the goal of employing them as a charge diagnostics in a plasma are based on the complex dielectric functions of the real materials [34,35]. In our work on topological aspects of light scattering by dielectric core-shell particles [33], we found, however, dissipation to blur higher-order bonding and antibonding resonances. For the present purpose, we employ, therefore, dissipationless model dielectric functions with parameters chosen such that bonding and antibonding resonances can be clearly identified up to the third multipole order.

As in our work on topological aspects of light scattering by dielectric core-shell particles [33], we set $N_m = 1$, that is, embed the particle in vacuum, and use

$$\varepsilon' = \varepsilon_\infty + \lambda_{TO}^{-2}\frac{\varepsilon_0 - \varepsilon_\infty}{\lambda_{TO}^{-2} - \lambda^{-2}}, \quad \varepsilon'' = 0, \tag{30}$$

with λ_{TO}^{-1} the wave number of the transverse optical phonon, and ε_0 and ε_∞ the dielectric constants at large and small wave numbers, given in Table I for the core and the shell, respectively. The real parts of the model dielectric functions are shown in Fig. 2. Of particular interest is the spectral range where surface modes at the core-shell interface are excited, that is, the range of wave numbers where the real part of the dielectric function of the shell is negative and the real part of the dielectric function of the core is positive. For the model dielectric functions plotted in Fig. 2, this is the case for $600\ \text{cm}^{-1} < \lambda^{-1} < 1900\ \text{cm}^{-1}$.

The resonances in this spectral range are depicted in Fig. 3 as a function of the filling factor $f = r_1/r_2$ for a particle with radius $r_2 = 0.6\ \mu$m. In accordance with the hybridization scenario [28–30] and our previous work [33,34], we label the resonances at lower wave numbers bonding (subscript A) and the resonances at higher wave numbers antibonding (subscript B). Justification for this labeling comes from the polarities of

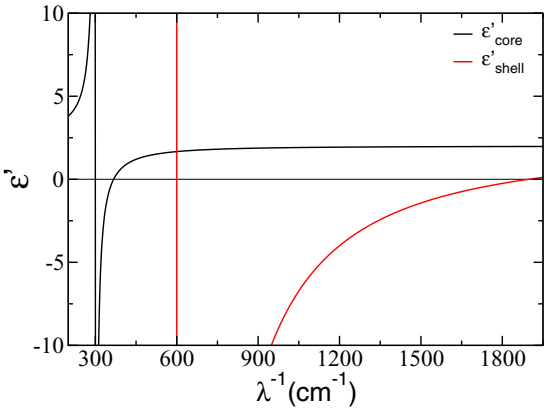

FIG. 2. Real parts of the dielectric functions specified by Eq. (30) and the parameters in Table I as a function of the wave number λ^{-1}.

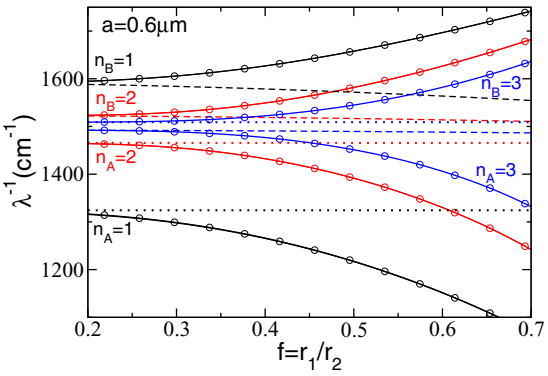

FIG. 3. Solid lines show the wave numbers of the bonding (subscript A) and antibonding (subscript B) dipole ($n_{A,B} = 1$), quadrupole ($n_{A,B} = 2$), and hexapole ($n_{A,B} = 3$) resonance as a function of the filling factor $f = r_1/r_2$ for a core-shell particle with radius $r_2 = 0.6\ \mu$m. The dotted and dashed lines denote, respectively, the positions of the resonances of the medium-embedded homogeneous shell particle and the shell-embedded core cavity, while bullets indicate the positions of the maxima in the extinction spectrum.

the induced surface charges at the two interfaces which are in-phase for the bonding and out-of-phase for the antibonding resonances [33]. The solid lines give the positions for the bonding and antibonding dipole ($n_{A,B} = 1$), quadrupole ($n_{A,B} = 2$), and hexapole ($n_{A,B} = 3$) resonance as obtained from the poles of Eq. (21), while the dotted and dashed lines give, respectively, the solutions of Eqs. (23) and (24), that is, the positions of the resonances of the medium-embedded homogeneous shell particle and the shell-embedded core cavity. Also shown are the positions of the maxima in the extinction efficiency, $Q_t = \frac{2}{x_2}\sum_{n=1}^{\infty}(2n+1)\text{Re}[a_n^m + b_n^m]$, where a_n^m and b_n^m are the expansion coefficients of the scattered fields $\vec{E}_s^m$ and $\vec{H}_s^m$ [see Eqs. (4) and (5)]. The resonances in the extinction spectrum depicted by the bullets follow precisely the resonances in the expansion coefficients d_n^2 and a_n^2, indicating that the denominator of a_n^m, which is the resonant coefficient in the expansion of the scattered fields, can be written in the same form as the denominators of d_n^2 and a_n^2.

The main feature of Fig. 3 is the increasing splitting between the bonding and antibonding resonances with increasing filling factor $f = r_1/r_2$. As expected from the hybridization scenario, the hybridization strength $X_n^{\text{cpl}}(x_1)Z_n^2(x_2)$ controlling the splitting increases with f because the decrease in shell thickness leads to a stronger coupling between the surface modes at the core-shell and the shell-medium interface. For $f \approx 0.2$, the resonances of the core-shell particle merge with the resonances of its building blocks, implying that the hybridization strength becomes vanishingly small. Notice that for $n_{A,B} \leqslant 2$, the bonding resonances merge with the resonances of the medium-embedded homogeneous shell particle, that is, the solutions of $E_n^2(x_2) = 0$, while the antibonding resonances merge with the resonances of the shell-embedded core cavity, that is, the solutions of $E_n^1(x_1) = 0$. For $n_{A,B} = 3$, however, it is the other way around. The reason is simply the energetic ordering of the resonances of the building blocks. For $n_{A,B} \leqslant 2$, the resonances of the shell-embedded core cavity are energetically above the resonances of the medium-embedded homogeneous

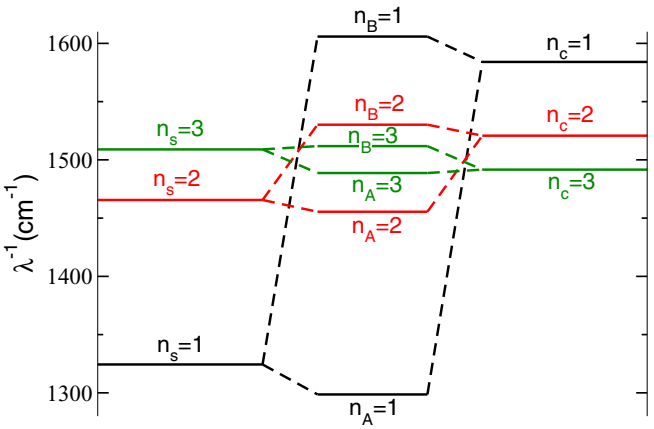

FIG. 4. Energetic positions of the resonances of the medium-embedded homogeneous shell particle ($n_s = 1,2,3$), the shell-embedded core cavity ($n_c = 1,2,3$), and the core-shell particle ($n_{A,B} = 1,2,3$) for $f = 0.3$ and $r_2 = 0.6$ μm. From the decreasing deviations of the hybridized from the noninteracting resonances can be inferred that the hybridization strength $X_n^{\mathrm{cp1}}(x_1)Z_n^2(x_2)$ decreases with increasing multipole order.

shell particle, while for $n_{\mathrm{A,B}} = 3$, the ordering is reversed. Figure 4 displays this ordering for $f = 0.3$.

Another way to visualize the hybridization scenario for the core-shell particle is to look at the electric fields inside the shell. This is shown in Fig. 5 for the dipole ($n = 1$), quadrupole ($n = 2$), and hexapole ($n = 3$) resonances of a particle with radius $r_2 = 0.6$ μm and filling factor $f = 0.3$. The lower and upper panels in Fig. 5 depict, respectively, the bonding and antibonding resonances. The correctness of the assignment can be inferred from the black arrows visualizing the orientation of the electric field inside and outside the particle. From them, the polarity of the induced surface charges follows, verifying that it is in-phase for the bonding and out-of-phase for the antibonding resonances. The wave numbers are tuned to maximize the spatial extension of the scattered fields outside the particle, $\vec{E}_s^m$ and $\vec{H}_s^m$, taking as a measure the distance of the singular points [36,37] in the outer Poynting field from the center of the particle (for a discussion of singular points in the dipole fields of dielectric core-shell particles, see Ref. [33]). From the ratio of the intensity of the scattering electric field inside the shell $|\vec{E}_s^2|^2$ to the intensity of the overall electric field inside the shell $|\vec{E}_p^2 + \vec{E}_s^2|^2$, shown by the color coding, it can, moreover, be deduced that the influence of the scattering fields is for the antibonding hexapole resonance smaller than for the bonding one, in contrast to the dipole and quadrupole resonances where it is reversed. The reason is again the energetic ordering of the resonances plotted in Fig. 4. The hexapole resonance of the shell-embedded core cavity drops below the hexapole resonance of the medium-embedded homogeneous shell particle. As a result, for $n = 3$, it is the bonding resonance which acquires more cavity character, and is thus more affected by the scattering fields, and not the antibonding one as it is the case for $n = 1,2$.

For core-shell particles with dissipation, having complex dielectric functions, the higher-order bonding and antibonding resonances may be blurred. For a CaO/Al_2O_3 particle, for instance, only the dipole and quadrupole resonances can be clearly identified [33]. Hence, higher-order bonding and antibonding resonances may be distinguishable only for

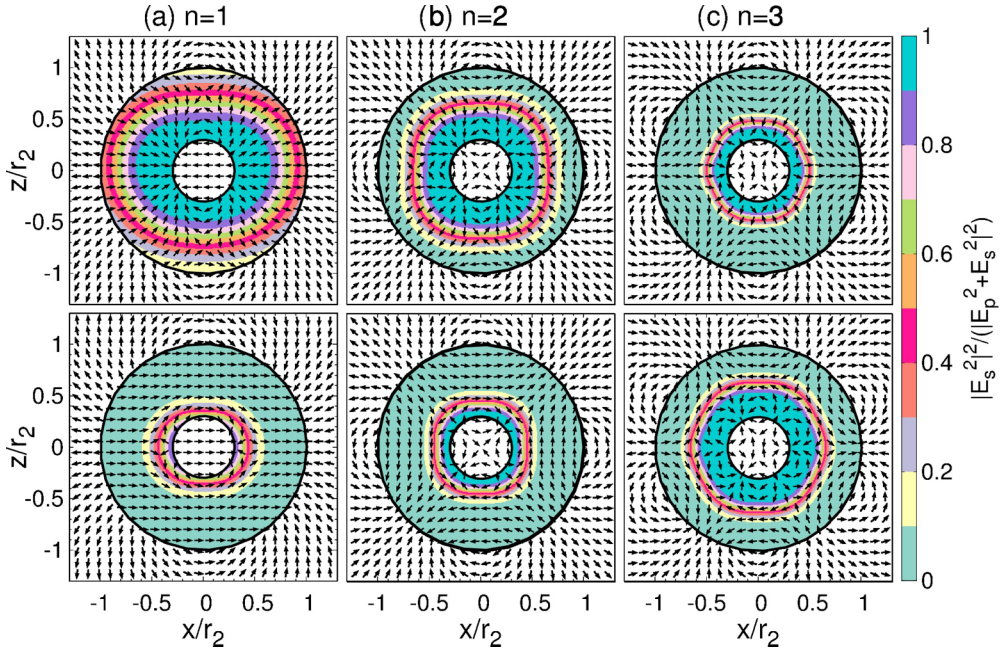

FIG. 5. Electric field distributions in the xz plane of a core-shell particle ($r_2 = 0.6$ μm, $f = 0.3$) near the bonding (lower panels) and antibonding (upper panels) dipole ($n = 1$), quadrupole ($n = 2$), and hexapole ($n = 3$) resonances. The wave numbers are $\lambda^{-1} = 1313.62$ cm^{-1} and $\lambda^{-1} = 1607.85$ cm^{-1} for the bonding and antibonding dipole, $\lambda^{-1} = 1455.5$ cm^{-1} and $\lambda^{-1} = 1530.22$ cm^{-1} for the bonding and antibonding quadrupole, and $\lambda^{-1} = 1488.706$ cm^{-1} and $\lambda^{-1} = 1511.805$ cm^{-1} for the bonding and antibonding hexapole resonance. The direction of the total electric field is shown by black arrows and the color coding gives the intensity of the scattering fields in units of the intensity of the overall electric fields inside the shell. Black circles indicate the particle and its core.

a judicious choice of materials. The multipole where the character of the bonding and antibonding resonance changes depends also on the materials. It can occur already for the dipole [14]. The character of the resonances determines the number and locations of the singular points as well as the spatial distribution of the dissipation inside the core-shell particle [33]. Changing it by tuning the resonances of its building blocks may thus be interesting from a physics and an application point of view.

IV. CONCLUSIONS

The hybridization scenario for the classical optical response of composite objects states that it can be understood in terms of interacting surface modes arising at the interfaces of the object.

For the particular case of a spherical core-shell particle, we derived the scenario directly from the expansion of the electromagnetic fields inside and outside the particle in terms of vector spherical harmonics. By reorganizing the fields inside the shell region into the penetrating fields of a shell particle and the scattered fields of a core cavity, we were able to derive formulas for the expansion coefficients resembling the diagonal elements of a matrix resolvent describing two hybridized energy levels. From the formulas, the building blocks of the hybridization scenario, i.e., the shell-embedded core cavity and the medium-embedded homogeneous shell particle, as well as the coupling between them could be straightforwardly identified. The physical content of the coefficients became thus immediately clear. In the Appendix, we also demonstrated that the same strategy can be applied to a stratified sphere containing an arbitrary number of shells. Reorganizing the expansion coefficients for the fields yields again expressions which resemble the diagonal elements of a matrix resolvent describing a chain of hybridized energy levels. The basic building blocks of the hybridization scenario and their coupling could thus be identified directly from the expansion coefficients.

Initially, the hybridization scenario has been deduced in the electrostatic approximation for small spherical stratified particles without retardation using equations for the surface charges induced at the interfaces. The derivation we presented includes retardation and is thus applicable to spherical stratified particles of any size. In addition, it provides a road map for analytically deriving the hybridization scenario for other composite objects with high symmetry for which analytical solutions of the Mie theory are available. The physical mechanisms buried in these solutions may thus become apparent.

ACKNOWLEDGMENTS

This work was supported by the Deutsche Forschungsgemeinschaft through the Transregional Collaborative Research Center SFB/TRR24.

APPENDIX

In this Appendix, we reorganize the Mie theory of a stratified spherical particle [18,21–23] to obtain the hybridization scenario for this situation also.

As indicated in Fig. 6, the particle contains k layers. The core is counted as the first layer $i = 1$, while the outermost

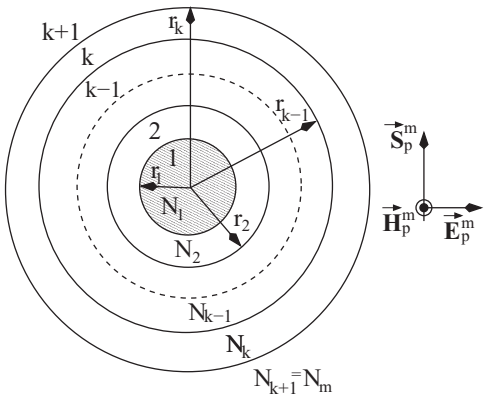

FIG. 6. Geometry of light scattering by a stratified sphere with total radius r_k containing k layers with radii r_i for $1 \leqslant i \leqslant k$, whereby the core is counted as the first layer ($i = 1$). Refractive indices N_i characterize each layer and the medium ($i = k + 1 = m$). The incident electromagnetic plane wave is described by a Poynting vector $\vec{S}_p^m$ propagating in the z direction, an electric field $\vec{E}_p^m$ polarized in the x direction, and a magnetic field $\vec{H}_p^m$ along the y direction.

layer and the surrounding medium are labeled $i = k$ and $i = k + 1 = m$, respectively. The label i is used for both the ith shell and its interface to the $(i + 1)$th shell. The abbreviations of the main text are adopted. Each layer i is characterized by its radius r_i, its magnetic permeability μ_i, and its refractive index $N_i(\lambda^{-1}) = \sqrt{\varepsilon_i(\lambda^{-1})}$, where $\varepsilon_i(\lambda^{-1}) = \varepsilon_i'(\lambda^{-1}) + i\varepsilon_i''(\lambda^{-1})$ is the complex dielectric function for the respective region. The total radius of the particle is the radius of the outermost layer r_k. As before, we use $k_i = \kappa N_i$ with $i = 1, \ldots, k, k + 1$, where $N_{k+1} = N_m$ is the refractive index of the surrounding medium, and the size parameters $x_i = 2\pi\lambda^{-1} r_i$.

The expansions for the incident and the scattered fields outside the particle as well as for the penetrating fields inside the core, given, respectively, by Eqs. (1) and (2), (4) and (5), and (6) and (7), remain the same, while the splitting of the fields (and their interpretation) in the shell of the core-shell particle, viz. Eq. (10), is now adopted to each shell $2 \leqslant i \leqslant k$ of the stratified sphere. Hence,

$$\vec{E}^i_{\text{shell}} = \vec{E}^i_{\text{s}} + \vec{E}^i_{\text{p}} \quad \text{and} \quad \vec{H}^i_{\text{shell}} = \vec{H}^i_{\text{s}} + \vec{H}^i_{\text{p}}, \tag{A1}$$

whereby the scattered fields of the $(i - 1)$th subsystem

$$\vec{E}^i_{\text{s}} = \sum_{n=1}^{\infty} E_n \left(i a^i_n \vec{N}^{(3)}_{e1n} - b^i_n \vec{M}^{(3)}_{o1n} \right), \tag{A2}$$

$$\vec{H}^i_{\text{s}} = \frac{k_i c}{\omega \mu_i} \sum_{n=1}^{\infty} E_n \left(i b^i_n \vec{N}^{(3)}_{o1n} + a^i_n \vec{M}^{(3)}_{e1n} \right) \tag{A3}$$

interact with the penetrating fields of the ith subsystem

$$\vec{E}^i_{\text{p}} = \sum_{n=1}^{\infty} E_n \left(c^i_n \vec{M}^{(1)}_{o1n} - i d^i_n \vec{N}^{(1)}_{e1n} \right), \tag{A4}$$

$$\vec{H}^i_{\text{p}} = -\frac{k_i c}{\omega \mu_i} \sum_{n=1}^{\infty} E_n \left(d^i_n \vec{M}^{(1)}_{e1n} + i c^i_n \vec{N}^{(1)}_{o1n} \right), \tag{A5}$$

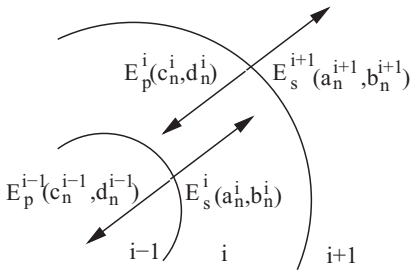

FIG. 7. Superposition of the electric fields in the shell region i. The resonance arising at the interface i between the ith and $(i+1)$th shell is characterized by a scattered field $\vec{E}_{\rm s}^{\,i+1}$ propagating into the $(i+1)$th shell and a field $\vec{E}_{\rm p}^{\,i}$ penetrating into the ith shell.

as schematically shown in Fig. 7. A resonance arising at the ith interface, which—in the counting scheme introduced above—separates the ith from the $(i+1)$th shell, is thus described by a scattered field propagating into the $(i+1)$th shell and a penetrating field propagating into the ith shell. The overall field in the ith shell is a superposition of the scattering fields of the $(i-1)$th subsystem and the penetrating fields of the ith subsystem.

Again, the expansion coefficients are determined by the electromagnetic boundary conditions. For the shell-medium interface at $r = r_k$,

$$\vec{r} \times \left(\vec{E}_{\rm p}^{k+1} + \vec{E}_{\rm s}^{k+1} - \vec{E}_{\rm s}^{k} - \vec{E}_{\rm p}^{k}\right) = 0, \tag{A6}$$

$$\vec{r} \times \left(\vec{H}_{\rm p}^{k+1} + \vec{H}_{\rm s}^{k+1} - \vec{H}_{\rm s}^{k} - \vec{H}_{\rm p}^{k}\right) = 0, \tag{A7}$$

while for the shell-shell interfaces at $r = r_i$ with $2 \leqslant i < k$,

$$\vec{r} \times \left(\vec{E}_{\rm s}^{i+1} + \vec{E}_{\rm p}^{i+1} - \vec{E}_{\rm s}^{i} - \vec{E}_{\rm p}^{i}\right) = 0, \tag{A8}$$

$$\vec{r} \times \left(\vec{H}_{\rm s}^{i+1} + \vec{H}_{\rm p}^{i+1} - \vec{H}_{\rm s}^{i} - \vec{H}_{\rm p}^{i}\right) = 0. \tag{A9}$$

The boundary conditions for the core-shell interface at $r = r_1$ remain Eqs. (17) and (18).

Before we identify the hybridization scenario from the expansion coefficients emerging from these boundary conditions, we recall that the Mie approach works with the expansion coefficients, whereas the hybridization scenario is an energetic picture focusing on energies (frequencies) for which the denominators of the expansion coefficients vanish. In deriving the energetic picture of the hybridization scenario from the expansion coefficients, the question arises therefore on which coefficient one should focus. It turns out that any coefficient becoming resonant in the considered parameter regime can be taken. A k-layered sphere containing k subsystems is described by the expansion coefficients c_n^i, b_n^{i+1}, d_n^i, and a_n^{i+1}, with $i = 1, \ldots, k$. To extract the hybridization scenario, we focus on d_n^i. It becomes resonant for small objects and is thus appropriate for our purpose.

Our guiding principle is again the mathematical structure of the diagonal elements of a matrix resolvent describing hybridized energy levels. Instead of two energy levels, appropriate for the core-shell particle, we now have to consider a resolvent for k energy levels. Generalizing the approach described in Sec. II, we thus have to rewrite d_n^i in a form resembling the diagonal elements of the matrix resolvent,

$$G(E) = \begin{pmatrix} \varepsilon_1 - E & V_{21} & 0 & \ldots & 0 \\ V_{21}^* & \varepsilon_2 - E & V_{32} & \ddots & \vdots \\ 0 & V_{32}^* & \ddots & \ddots & 0 \\ \vdots & \ddots & \ddots & \ddots & V_{kk-1} \\ 0 & \ldots & 0 & V_{kk-1}^* & \varepsilon_k - E \end{pmatrix}^{-1}, \tag{A10}$$

describing a chain of energy levels ε_i with nearest-neighbor interactions V_{ii-1}, where $i = 1, \ldots, k$ and $V_{10} = V_{k+1,k} = 0$. Using renormalized perturbation theory, they are given by [38] ($|i\rangle$ denotes the basis states)

$$G_i(E) = \langle i|G(E)|i\rangle = \cfrac{1}{g_i^{-1}(E) - \cfrac{|V_{i+1i}|^2}{g_{i+1}^{-1}(E) - \cfrac{|V_{i+2i+1}|^2}{\ddots - \cfrac{|V_{kk-1}|^2}{g_k^{-1}(E)}}} - \cfrac{|V_{ii-1}|^2}{g_{i-1}^{-1}(E) - \cfrac{|V_{i-1i-2}|^2}{\ddots - \cfrac{|V_{21}|^2}{g_1^{-1}(E)}}}}, \tag{A11}$$

where $g_i(E) = (E - \varepsilon_i)^{-1}$ is the resolvent of the ith noninteracting energy level. Its pole thus gives the energy of this level. The poles of $G_i(E)$, on the other hand, give the k excitation energies of the interacting system. Once the coefficient d_n^i is in this form, its interpretation along the lines of the hybridization scenario is obvious, as in the case of a core-shell particle.

Choosing all components nonmagnetic, that is, setting $\mu_i = 1$ for $i \leqslant k+1$, the coefficient d_n^i resulting from the boundary conditions can be indeed rewritten as

$$d_n^i = \cfrac{X_n^k(x_k) X_n^{k-1}(x_{k-1}) \cdots X_n^i(x_i) / \left[\tilde{E}_n^k(x_1, \cdots, x_k) \tilde{E}_n^{k-1,k}(x_1, \cdots, x_k) \cdots \tilde{E}_n^{i+1,i+2,\ldots,k}(x_1, \cdots, x_k)\right]}{E_n^i(x_i) - \cfrac{X_n^{{\rm cp}i}(x_1, \ldots, x_i) Z_n^{i+1}(x_{i+1})}{E_n^{i+1}(x_{i+1}) - \cfrac{X_n^{{\rm cp}i+1}(x_1, \ldots, x_{i+1}) Z_n^{i+2}(x_{i+2})}{\ddots - \cfrac{X_n^{{\rm cp}k-1}(x_1, \ldots, x_{k-1}) Z_n^k(x_k)}{E_n^k(x_k)}}} - \cfrac{X_n^{{\rm cp}i-1}(x_1, \ldots, x_{i-1}) Z_n^i(x_i)}{E_n^{i-1}(x_{i-1}) - \cfrac{X_n^{{\rm cp}i-2}(x_1, \ldots, x_{i-2}) Z_n^{i-1}(x_{i-1})}{\ddots - \cfrac{X_n^{{\rm cp}1}(x_1) Z_n^2(x_2)}{E_n^1(x_1)}}}}, \tag{A12}$$

that is, in a form closely resembling Eq. (A11). Obviously, E_n^i and $X_n^{{\rm cp}i-1} Z_n^i$ play, respectively, the role of g_i^{-1} and $|V_{ii-1}|^2$. The functions X_n^i and $\tilde{E}_n^{i,i+1,\ldots,k}$ in the numerator, having no direct analog, are irrelevant for our purpose as they are not involved in

the identification of resonance frequencies and coupling strengths. For better readability, we again present the definitions of all these functions when they enter the discussion of the physical content of Eq. (A12).

The analogy between a chain of k hybridized energy levels and the optical response of a k-layered sphere can be perhaps best seen by expressing Eq. (A12) as a diagonal element of a tridiagonal matrix. Suppressing the size parameters, Eq. (A12) can be written as

$$d_n^i = \frac{X_n^k X_n^{k-1} \cdots X_n^i}{\tilde{E}_n^k \tilde{E}_n^{k-1,k} \cdots \tilde{E}_n^{i+1,i+2,\ldots,k}} \langle i|M|i\rangle\,, \tag{A13}$$

with

$$M = \begin{pmatrix} E_n^1 & \sqrt{X_n^{\mathrm{cp}1} Z_n^2} & 0 & \cdots & 0 \\ \sqrt{X_n^{\mathrm{cp}1} Z_n^2} & E_n^2 & \sqrt{X_n^{\mathrm{cp}2} Z_n^3} & \ddots & \vdots \\ 0 & \sqrt{X_n^{\mathrm{cp}2} Z_n^3} & \ddots & \ddots & 0 \\ \vdots & \ddots & \ddots & \ddots & \sqrt{X_n^{\mathrm{cp}k-1} Z_n^k} \\ 0 & \cdots & 0 & \sqrt{X_n^{\mathrm{cp}k-1} Z_n^k} & E_n^k \end{pmatrix}^{-1}. \tag{A14}$$

Comparing (A14) with (A10), it becomes clear that the optical response of a k-layered particle can be interpreted in terms of k hybridized subsystems with individual resonances determined by $(i = 1, \ldots, k)$

$$\begin{aligned} E_n^i(x_i) &= N_i \xi_n'(N_{i+1}x_i)\psi_n(N_i x_i) - N_{i+1}\xi(N_{i+1}x_i)\psi_n'(N_i x_i) \\ &= 0, \end{aligned} \tag{A15}$$

and hybridization strengths given by $X_n^{\mathrm{cp}i-1}(x_1, \ldots, x_{i-1})$ $Z_n^i(x_i)$. Notice in Eq. (A15) the implicit definition of the function $E_n^i(x_i)$, which also appears in Eq. (A12). Clearly, Eq. (A15) is the resonance condition of a homogeneous particle with size parameter x_i and refractive index N_i embedded in a medium specified by N_{i+1}.

We now turn to the hybridization strength of the subsystem i, which, in contrast to the core-shell particle, interacts with two adjacent subsystems. The interaction with the $(i-1)$th and the $(i+1)$th subsystem is given by $X_n^{\mathrm{cp}i-1}(x_1, \ldots, x_{i-1})Z_n^i(x_i)$ and $X_n^{\mathrm{cp}i}(x_1, \ldots, x_i)Z_n^{i+1}(x_{i+1})$, respectively. Here,

$$Z_n^i(x_i) = N_i \xi_n'(N_{i+1}x_i)\xi_n(N_i x_i) - N_{i+1}\xi_n(N_{i+1}x_i)\xi_n'(N_i x_i), \tag{A16}$$

for $i = 2, \ldots, k$, and

$$\begin{aligned} &X_n^{\mathrm{cp}i}(x_1, \ldots, x_i) \\ &\quad = X_n^{\mathrm{p}i}(x_i) + \frac{X_n^{\mathrm{cp}i-1}(x_1, \ldots, x_{i-1})U_n^i(x_i)}{E_n^{1,\ldots,i-1}(x_1, \ldots, x_{i-1})}, \end{aligned} \tag{A17}$$

for $i = 1, \ldots, k-1$, with $X_n^{\mathrm{cp}0} = 0$. The functions in the definition of $X_n^{\mathrm{cp}i}$ are

$$\begin{aligned} X_n^{\mathrm{p}i}(x_i) &= N_i \psi_n'(N_{i+1}x_i)\psi_n(N_i x_i) \\ &\quad - N_{i+1}\psi_n(N_{i+1}x_i)\psi_n'(N_i x_i), \end{aligned} \tag{A18}$$

$$U_n^i(x_i) = N_{i+1}\psi_n(N_{i+1}x_i)\xi_n'(N_i x_i) - N_i \psi_n'(N_{i+1}x_i)\xi_n(N_i x_i), \tag{A19}$$

and

$$\begin{aligned} &E_n^{1,\ldots,i}(x_1, \ldots, x_i) \\ &\quad = E_n^i(x_i) + \frac{X_n^{\mathrm{cp}i-1}(x_1, \ldots, x_{i-1})Z_n^i(x_i)}{E_n^{1,\cdots,i-1}(x_1, \ldots, x_{i-1})}, \end{aligned} \tag{A20}$$

where $E_n^i(x_i)$ is defined in Eq. (A15). The function $X_n^{\mathrm{cp}i}$ depends on the size parameters $x_1, \ldots, x_i$. Its superscript cp$i$, standing for composed, propagating, and ith shell, distinguishes it from the function $X_n^{\mathrm{p}i}$ which depends only on the size parameter x_i. The recursion (A20) generates the second continued fraction in the denominator of Eq. (A12).

Of interest is also under what conditions the ith subsystem of the stratified sphere can be isolated and how this affects the expansion coefficient d_n^i. The decoupling is a two-step process. In a first step, the interaction with the outer subsystems is turned off by choosing the outer shells and the embedding medium to be identical to the $(i+1)$th shell, that is, setting $N_j = N_{i+1}$ for $i+1 < j \leqslant k+1$, which leads to $Z_n^j(x_j) = 0$ for $i+1 \leqslant j \leqslant k$. In a second step, we turn off the interaction between the inner subsystems by choosing the refractive indices of the internal layers j for $j < i$ and the refractive index of the ith layer to be the same. Hence, $N_j = N_i$ for $j < i$, so that $X_n^{\mathrm{cp}i-1}(x_1, \ldots, x_{i-1}) = 0$. To analyze how the isolation of the ith subsystem affects the expansion coefficient d_n^i, we need also to look at the functions

$$\begin{aligned} X_n^i(x_i) &= N_i \psi_n(N_{i+1}x_i)\xi_n'(N_{i+1}x_i) \\ &\quad - N_i \psi_n'(N_{i+1}x_i)\xi_n(N_{i+1}x_i) \end{aligned} \tag{A21}$$

and

$$\begin{aligned} &\tilde{E}_n^{i,i+1,\ldots,k}(x_1, \ldots, x_k) \\ &\quad = E_n^i(x_i) + \frac{X_n^{\mathrm{cp}i}(x_1, \ldots, x_i)Z_n^{i+1}(x_{i+1})}{\tilde{E}_n^{i+1,i+2,\ldots,k}(x_1, \ldots, x_k)} \end{aligned} \tag{A22}$$

entering the numerator in Eq. (A12). The functions $E_n^i(x_i), Z_n^i(x_i)$, and $X_n^{\mathrm{cp}i}(x_1, \ldots, x_i)$ are defined in Eqs. (A15), (A16), and (A17), respectively. Note that the

recursion (A22) defines the first continued fraction in the denominator of (A12). Due to the decoupling, that is, the particular identification of refractive indices, the interaction term $X_n^{\mathrm{cpi}}(x_1,\ldots,x_i)Z_n^{i+1}(x_{i+1})$ in Eq. (A22) vanishes, leading to $\tilde{E}_n^{i,\cdots,k}(x_1,\ldots,x_k)=E_n^i(x_i)$. In addition, $X_n^j(x_j)/E_n^j(x_j)=1$ for $j>i$. Thus, Eq. (A12) becomes

$$d_n^i=\frac{X_n^i(x_i)}{E_n^i(x_i)}, \tag{A23}$$

with $X_n^i(x_i)$ and $E_n^i(x_i)$ given by Eqs. (A21) and (A15).

Due to the decoupling, d_n^i should be attached to the penetrating fields inside a homogeneous particle characterized by N_i embedded in a medium with the refractive index N_{i+1}. Indeed, looking at the penetrating coefficient of a homogeneous sphere given by Eq. (28) and substituting $N_m\to N_{i+1}, N_2\to N_i$, and $x_2\to x_i$ makes (28) identical to (A23). Hence, if $N_j=N_i$ for all $j<i$ and $N_j=N_{i+1}$ for all $j>i+1$, then the k-layered particle is reduced to a homogeneous particle with radius r_i embedded in a medium, whereby the used materials are described by N_i and N_{i+1}, respectively.

As in the case of the core-shell particle, the original expansion coefficients of a k-layered sphere [21–24] reduce in the respective limits also to the coefficients of the subsystems. Due to the rewriting, we demonstrate, however, that the subsystems are always virtually present. The rewriting thus identifies the limiting subsystems as basic building blocks whose coupling yields the unique optical response of the composite object.

[1] G. Mie, Ann. Phys. (Leipzig) **330**, 377 (1908).
[2] P. Debye, Ann. Phys. (Leipzig) **335**, 57 (1909).
[3] M. Kerker, *The Scattering of Light and Other Electromagnetic Radiation* (Academic, San Diego, 1969).
[4] C. F. Bohren and D. R. Huffman, *Absorption and Scattering of Light by Small Particles* (Wiley, New York, 1983).
[5] J. E. Hansen and L. D. Travis, Space Sci. Rev. **16**, 527 (1974).
[6] S. A. Maier and H. A. Atwater, J. Appl. Phys. **98**, 011101 (2005).
[7] X. Fan, W. Zheng, and W. J. Singh, Light: Sci. Appl. **3**, e179 (2014).
[8] F. Kretschmer, S. Mühlig, S. Hoeppner, A. Winter, M. D. Hager, C. Rockstuhl, T. Pertsch, and U. S. Schubert, Part. Part. Syst. Charact. **31**, 721 (2014).
[9] N. J. Halas, S. Lal, S. Link, W.-S. Chang, D. Natelson, J. H. Hafner, and P. Nordlander, Adv. Mater. **24**, 4842 (2012).
[10] T. C. Preston and R. Signorell, Acc. Chem. Res. **45**, 1501 (2012).
[11] H. Wang, D. W. Brandl, F. Le, P. Nordlander, and N. J. Halas, Nano Lett. **6**, 827 (2006).
[12] J. Aizpurua, P. Hanarp, D. S. Sutherland, M. Käll, G. W. Bryant, and F. J. García de Abajo, Phys. Rev. Lett. **90**, 057401 (2003).
[13] S. J. Oldenburg, R. D. Averitt, S. L. Westcott, and N. J. Halas, Chem. Phys. Lett. **288**, 243 (1998).
[14] R. Bardhan, N. K. Grady, T. Ali, and N. J. Halas, ACS Nano **4**, 6169 (2010).
[15] C. Loo, A. Lin, L. Hirsch, M.-H. Lee, J. Barton, N. Halas, J. West, and R. Drezek, Technol. Cancer Res. Treat. **3**, 33 (2004).
[16] J. R. Cole and N. J. Hallas, Appl. Phys. Lett. **89**, 153120 (2006).
[17] A. L. Aden and M. Kerker, J. Appl. Phys. **22**, 1242 (1951).
[18] J. R. Wait, Appl. Sci. Res. B **10**, 441 (1962).
[19] R. Ruppin, Surf. Sci. **51**, 140 (1975).
[20] C. Uberoi, Phys. Lett. A **76**, 69 (1980).
[21] R. Bhandari, Appl. Opt. **24**, 1960 (1985).
[22] J. Sinzig and M. Quinten, Appl. Phys. A **58**, 157 (1994).
[23] H. Xu, Phys. Rev. B **72**, 073405 (2005).
[24] O. Peña and U. Pal, Comput. Phys. Commun. **180**, 2348 (2009).
[25] T. Wriedt, Part. Part. Syst. Charact. **15**, 67 (1998).
[26] N. T. Zakharova, G. Videen, and N. G. Khlebtsov, J. Quantum Spectrosc. Radiat. Transfer **113**, 1844 (2012).
[27] N. G. Khlebtsov, J. Quantum Spectrosc. Radiat. Transfer **123**, 184 (2013).
[28] E. Prodan, C. Radloff, N. J. Halas, and P. Nordlander, Science **302**, 419 (2003).
[29] E. Prodan and P. Nordlander, J. Chem. Phys. **120**, 5444 (2004).
[30] T. C. Preston and R. Signorell, Proc. Natl. Acad. Sci. USA **108**, 5532 (2011).
[31] C. Radloff and N. J. Halas, Nano Lett. **4**, 1323 (2004).
[32] M. R. Jones, K. D. Osberg, R. J. Macfarlane, M. R. Langille, and C. A. Mirkin, Chem. Rev. **111**, 3736 (2011).
[33] E. Thiessen, F. X. Bronold, R. L. Heinisch, and H. Fehske, Phys. Rev. A **91**, 043837 (2015).
[34] E. Thiessen, R. L. Heinisch, F. X. Bronold, and H. Fehske, Eur. Phys. J. D **68**, 98 (2014).
[35] R. L. Heinisch, F. X. Bronold, and H. Fehske, Phys. Rev. Lett. **109**, 243903 (2012).
[36] Z. B. Wang, B. S. Luk'yanchuk, M. H. Hong, Y. Lin, and T. C. Chong, Phys. Rev. B **70**, 035418 (2004).
[37] M. I. Tribelsky and B. S. Lyk'yanchuk, Phys. Rev. Lett. **97**, 263902 (2006).
[38] E. N. Economou and M. H. Cohen, Phys. Rev. B **4**, 396 (1971).